# Enhancement of optically pumped spin orientation via spin-exchange collisions at low vapor density

W. Chalupczak,[1] R. M. Godun,[1] P. Anielski,[2] A. Wojciechowski,[2] S. Pustelny,[2,3] and W. Gawlik[2]
[1]*National Physical Laboratory, Hampton Road, Teddington TW11 0LW, United Kingdom*
[2]*Center for Magneto-Optical Research, M. Smoluchowski Institute of Physics, Jagiellonian University, Reymonta 4, PL 30-059 Kraków, Poland*
[3]*Department of Physics, University of California at Berkeley, Berkeley, California 94720-7300, USA*
(Received 13 February 2012; published 4 April 2012)

An effect is demonstrated where off-resonant optical pumping is enhanced by spin-exchange collisions, which enables a high degree of spin orientation to be obtained in alkali-metal atoms. The experiment with room-temperature cesium vapor employs radio-frequency spectroscopy under conditions of the nonlinear Zeeman effect that allow the populations of the individual Zeeman sublevels to be determined. The improved efficiency of atomic orientation leads to a significant reduction of population relaxation out of the state with maximum magnetic quantum number $m$ (stretched state), which is observed as a narrowing of radio-frequency resonances. Spin-exchange collisions play a crucial role in this effect although the applied atomic density $\sim 10^{11}$ cm$^{-3}$ corresponds to collision rates not greater than several tens of Hz. A simplified theoretical model has been developed to reproduce the measurement results numerically.

DOI: 10.1103/PhysRevA.85.043402 PACS number(s): 32.60.+i, 42.65.−k

## I. INTRODUCTION

Spin-exchange collisions (SEC) influence the results of many precision measurements [1]. In the field of cold atoms, for example, the accuracy of primary frequency standards based on atomic fountains was limited for almost a decade by the estimated uncertainty of the collisional frequency shift [2]. The demonstration of Bose-Einstein condensation in cesium atoms proved to be difficult due to the unusually high rate of inelastic collisions [3]. In thermal atomic samples, the presence of SEC on the one hand creates a relaxation channel that usually decreases the sensitivity of atomic magnetometers [4], yet on the other hand constitutes the essential ingredient for the spin-exchange optical pumping technique utilized in the generation of polarization in noble gas samples [5].

For the case of unfavorable influences of SEC on thermal ensembles, the main strategy to minimize the number of inelastic collisions involves operation with a low-density vapor ($<10^{12}$ cm$^{-3}$) in a paraffin-coated glass cell [6]. Alternatively, it has been observed by Happer and Tang [7] that the relaxation rate can also be decreased for atomic densities above $10^{13}$ cm$^{-3}$ in low magnetic fields by exploiting the rapid spin oscillations that result from frequent collisions [4]. Systematic studies of the effects of SEC in a high-density alkali-metal vapor were described in Ref. [8]. Another approach to reduce collisional relaxation relies on the generation of orientation (vector polarization) in atoms, by the optical pumping to the stretched state, i.e., the state with the maximum or minimum magnetic quantum number $m$ [9,10]. Collisions of atoms in such states do not introduce spin-exchange relaxation as the total angular momentum must be conserved in this process. For the stretched states, this leaves no opportunity for the colliding atoms to move to any other states.

A standard method for pumping alkali-metal atoms to the stretched state employs a circularly polarized laser beam operating on the $D_1$ line [11]. For even more efficient pumping, an additional laser, the so-called repumper, is added to transfer the atoms from the other hyperfine ground state [12]. One serious disadvantage of this approach for radio-frequency (rf) spectroscopy is the power broadening occurring due to the resonant optical interaction with states involved in the rf transitions [8,13].

This paper demonstrates a way of generating a high level of orientation in the ground state (up to 92%), and reducing the population relaxation arising from SEC in a low-density ($\sim 10^{11}$ cm$^{-3}$) cesium vapor. The orientation of the $F = 4$ ground-state Zeeman sublevels is achieved indirectly, as a consequence of a direct orientation of the $F = 3$ states and SEC [Fig. 1(a)]. Our experiments reveal the existence of two regimes of pump-beam intensity, where SEC influence the result of optical pumping in two different ways. In the regime of low light intensity, SEC are responsible mostly for equalizing the degree of orientation among all atoms, regardless of the hyperfine manifold they occupy. This occurs by effectively transferring the orientation created in the $F = 3$ manifold to the $F = 4$ manifold. In the regime of high light intensity, however, a strong enhancement of the orientation is observed due to SEC aiding the pumping process.

The indirect orientation in the $F = 4$ manifold and, in particular, the absence of direct optical coupling of the pump beam to the $F = 4$ sublevels enables observation of the narrowing of the relevant rf resonances. The results of this paper show both experimentally and theoretically how the orientation builds up in the $F = 4$ state, and how the newly proposed method reduces perturbation of the $F = 4, m = -4$ sublevel.

The combination of high orientation and narrow resonance lines is beneficial for many precision measurements; in particular, the presented technique creates an opportunity for enhanced sensitivity of rf magnetometers, and allows simplification of the measurement instrumentation. Indirect orientation has been recently discussed by Scholtes *et al.* [14]. In contrast to our experiment with the atomic sample at ambient temperature, however, the experiment of Ref. [14] was performed at a much higher temperature of about 135 °C, in an atmosphere of 170 mbar of nitrogen as a quenching gas, and in a relatively small magnetic offset field (5 $\mu$T).

 

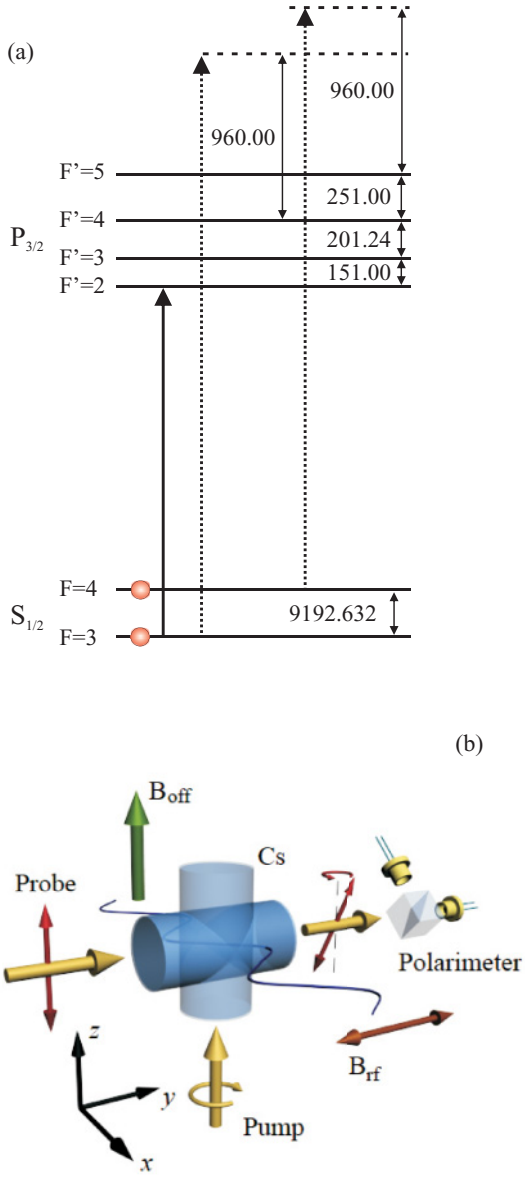


FIG. 1. (Color online) (a) Energy structure of the cesium $6\,^2S_{1/2} \rightarrow 6\,^2P_{3/2}$ transition ($D_2$ line, 852 nm). The solid arrow represents the frequency of the beam generating the orientation, while the dashed arrows represent the relevant frequencies of the probe laser used in the experiments. (b) Geometry of the experiment. A circularly polarized laser beam propagating along the $z$ axis optically pumps the sample of Cs atoms contained in a paraffin-coated glass cell. A linearly polarized probe beam propagates along the $y$ direction. The polarization of the probe light is parallel to $B_{\rm off}$. The polarization state of the light after traversing the atomic sample is measured with a balanced polarimeter. The oscillating field $B_{\rm rf}$ oriented orthogonally to $B_{\rm off}$ creates oscillations of the polarization plane of the probe beam.

This paper describes the experimental conditions in Sec. II, presents the results of the measurements and theoretical modeling in Sec. III, and gives the conclusions in Sec. IV.

## II. EXPERIMENTAL SETUP

The experimental setup is represented schematically in Fig. 1(b). A sample of thermal Cs atoms is placed in a highly uniform static magnetic (offset) field aligned along the $z$ axis ($B_{\rm off}$). An additional pair of coils generates a weak rf magnetic field oscillating along the $y$ direction. The ambient magnetic field is suppressed by the use of five layers of cylindrical shields made from 2-mm-thick mu-metal with end caps (static shielding better than $3 \times 10^6$ and the residual relative field gradients over the cell length are $<10^{-5}$).

The atomic vapor is housed in an antirelaxation, paraffin-coated, cross-shaped glass cell (diameter of 22 mm, arm length of 22 mm), with a stem containing metal droplets attached to the center of the cross. The stem can be heated to increase the atomic density by a temperature-controlled water flow around the whole cell.

The sample is optically pumped by a circularly polarized ($\sigma^-$) laser beam propagating along $B_{\rm off}$. The beam is generated by an external-cavity diode laser, frequency locked to the cesium $D_2$ line (852 nm) using a Doppler-free dichroic lock technique [16], and additionally monitored with a standard saturated-absorption setup. The exact tuning point is in the vicinity of the $S_{1/2}F = 3 \rightarrow P_{3/2}F' = 2$ transition, though this tuning was later varied and examined in the full range of the $S_{1/2}F = 3 \rightarrow P_{3/2}F'$ transitions. The pump-beam diameter is 20 mm, covering the whole volume of the vapor cell.

A second probe beam is linearly polarized parallel to z and propagates along the $y$ axis, orthogonally to the magnetic field. It is provided by a tapered amplifier operating also on the $D_2$ line, frequency stabilized either to the $S_{1/2}F = 4 \rightarrow P_{3/2}F' = 5$ or to the $S_{1/2}F = 3 \rightarrow P_{3/2}F' = 4$ transitions using a standard saturated-absorption setup, and subsequently frequency shifted by 960 MHz to the blue by two acousto-optic modulators in a double-pass configuration. This nonresonant probing is essential for the reduction of power broadening in a way similar to that applied with the alignment configuration in Ref. [15]. The diameter of the probe beam is approximately 2 mm.

The population distribution of the ground-state Zeeman sublevels is studied by rf resonance spectroscopy [15]. This relies on the interaction of the atomic populations and coherences between adjacent Zeeman sublevels with an applied rf magnetic field in a way that can be monitored by observation of polarization rotation of a linearly polarized probe beam. The rotation is analyzed by a balanced polarimeter and the resulting signal is processed by either a lock-in amplifier or an rf spectrum analyzer. The experiment was performed with rf and probe beam powers sufficiently low that they had no noticeable effect on the pumping process. No effect of the pump-beam diameter was observed either.

For our study of the optical pumping and SEC, it is essential that the experiment is performed in a bias field $B_{\rm off}$ sufficiently strong that the nonlinear Zeeman effect lifts the degeneracy of the rf resonances between the neighboring Zeeman sublevels. Under such conditions, sweeping the frequency of the rf field allows one to record the spectra consisting of a series of resolved peaks (shown as insets to Fig. 2).

## III. RESULTS AND INTERPRETATION

### A. Resonance amplitudes, populations, and pumping efficiency

Let us first consider the pumping efficiency toward the target stretched state $F = 4$, $m = -4$ as a function of the

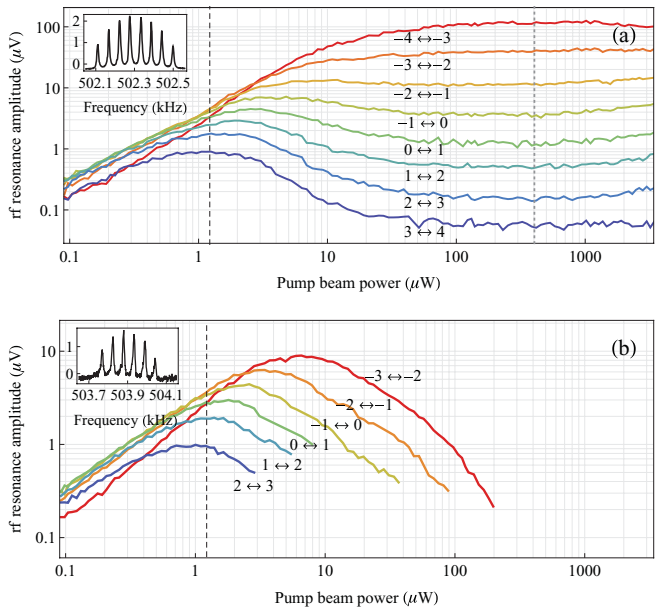


FIG. 2. (Color online) Amplitudes, $A^{|F,m\rangle\leftrightarrow|F,m+1\rangle}$, of the rf resonances corresponding to the transitions between successive magnetic sublevels ($m \leftrightarrow m' = m + 1$) in the (a) $F = 4$ and (b) $F = 3$ ground states versus the pump-beam power. Vertical dashed lines separate the low- and high-intensity regimes; the dotted line at about 400 $\mu$W marks the center of the power range with the highest orientation. Insets show rf spectra taken at 0.1 $\mu$W. The peaks from left to right represent the resonances (4,3), (3,2), (2,1), (1,0), (0,−1), (−1,−2), (−2,−3), (−3,−4) for $F = 4$ and (3,2), (2,1), (1,0), (0,−1),(−1,−2), (−2,−3) for $F = 3$.

pump-beam power. Figure 2 presents the measured amplitudes of the peaks observed in the rf spectra for pump-light powers ranging from 0.1 $\mu$W to 3 mW and its frequency tuned in a way that maximizes the rf signal amplitude (14 MHz below the $F = 3 \rightarrow F' = 2$ transition; see Sec. III C for the pump-beam tuning considerations). The amplitude of each peak is related to the population difference between neighboring Zeeman sublevels [13,17], and allows deduction of the population distribution established at a given pumping intensity level [see the discussion below; Eq. (1)].

### 1. *Low-intensity regime*

The insets of Fig. 2 show the rf spectra with a number of well-resolved peaks, which are observed with a pump power of ∼0.1 $\mu$W. Each peak of positive amplitude occurring in the presented rf spectra designates a rising gradient of population distribution among Zeeman sublevels of the relevant ground-state manifold. Even for such low powers, light significantly alters the population distribution in the ground states. Interestingly, the gradient in the $F = 3$ state, which is directly coupled to the pump light, and the one in the uncoupled $F = 4$ state reveal similar, roughly linear growth with increasing light power in the range of 0.1–1 $\mu$W.

Although the generation of a population gradient in the light coupled $F = 3$ state is to be expected (standard optical pumping), the appearance of the strong nonequilibrium population distribution in the other state is nontrivial. The $F = 4$ state is not coupled to light (the 9 GHz detuning of the light reduces the optical excitation) and its population distribution is barely modified by spontaneous emission from the $F' = 2,3,4$ states, since (a) $F' = 2 \rightarrow F = 4$ is a forbidden transition, (b) excitation of the $F' = 3$ state is hindered by a 165 MHz detuning and further reduced by the branching ratio (only 1/4 toward $F = 4$) [18], and (c) excitation of the $F' = 4$ state is negligible due to the 367 MHz detuning. Although the latter two transitions can be generated more efficiently at higher light power, for low intensities the optical pumping should be considered as operating only within the closed $F = 3 \rightarrow F' = 2$ transition. Consequently, if the regular optical pumping in the closed system were the only mechanism altering atomic populations, only the $F = 3$ sublevel populations would be affected and the $F = 4$ sublevels should be regarded as unperturbed by any optical process. This would result in a population distribution such as represented schematically in Fig. 3(a) with a flat distribution in the $F = 4$ manifold. On the contrary, the observed populations of the $F = 4$ sublevels clearly exhibit a nonuniform distribution which replicates the one present in the $F = 3$ manifold.

The observation of a population gradient in the $F = 4$ state may be explained as follows. Light generates orientation among the atoms in the $F = 3$ ground state [Fig. 3(a)]. SEC, involving all atoms, then distribute the overall angular momentum (or orientation) among both hyperfine manifolds [5,19]. We will refer to this process as SEC replication [see Fig. 3(b)]. This mechanism is similar to transferring spin polarization from optically pumped alkali-metal atoms to noble gas atoms in a spin-exchange optical pumping technique [5].

### 2. *High-intensity regime*

For pump-beam powers exceeding 1 $\mu$W the process described above needs to be reconsidered. In this case, the non-negligible probability of the $F = 3 \rightarrow F' = 3,4$ transitions drastically modifies the dynamics of the system by transferring population toward the $F = 4$ manifold [Fig. 3(c)]. It results in a reduction of the amplitudes of the rf resonances observed in the $F = 3$ state as its population is removed. One might expect a complementary behavior for the other hyperfine manifold, i.e., an increase of all the resonances in the $F = 4$ group. Interestingly, the experimental data shows that only the most dominant resonances follow this prediction and demonstrate a continuous amplitude growth (Fig. 2).

The rapid decline of the other amplitudes needs an additional explanation, which again is based on the SEC mechanism. This time, however, SEC operate under different conditions and reveal new features. Strong optical transfer disturbs the population balance between the two hyperfine manifolds such that occupation of the $F = 4$ manifold exceeds that of the $F = 3$. This results in an intense collisional population transfer $F = 4 \rightarrow F = 3$ continuously competing with the optical transfer. However, this collisional transfer features some essential selectivity. In the case of SEC, not all of the $F = 4$ ground-state sublevels are equally prone to be brought back to the $F = 3$ manifold as the effective SEC relaxation rates vary significantly between various sublevels. In particular, the relaxation of the stretched state becomes much slower than the decay of the nonstretched states for the polarized media [9].

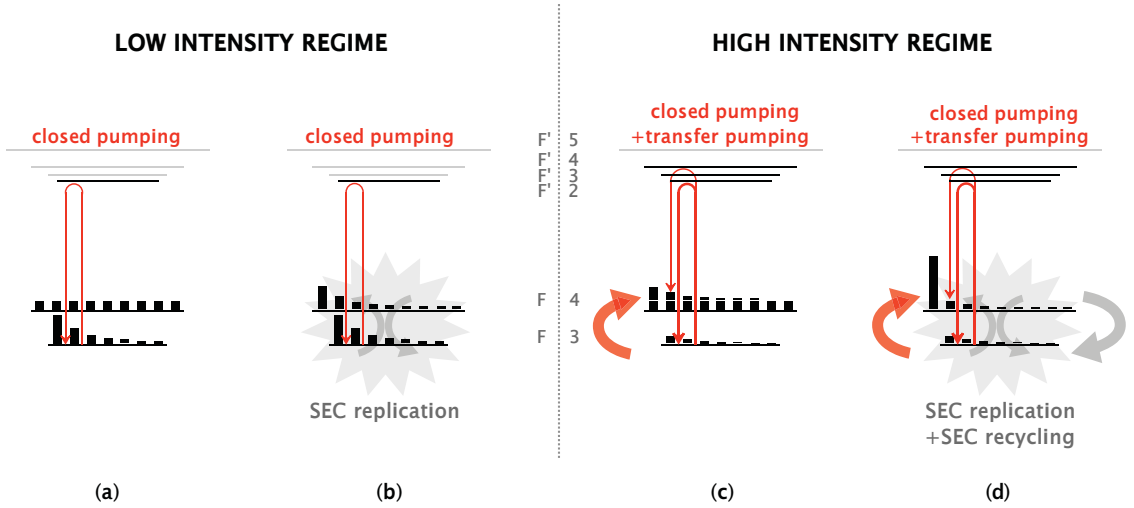


FIG. 3. (Color online) Schematic illustration of the distinct SEC contributions to the optical pumping mechanism for the two light-intensity regimes. Diagrams (a) and (c) show the hypothetical cases with no SEC mechanisms included.

An atom which is moved from the $F = 4$ to the $F = 3$ manifold is subsequently subjected to the intense optical pumping process involving several pumping cycles over the closed $F = 3 \rightarrow F' = 2$ transition before having a chance to be transferred back into the $F = 4$ manifold. There again it is most likely to be returned to the $F = 3$ manifold by SEC and the process repeats until the atom finally reaches the stretched state in $F = 4$. Once there, it is preserved from SEC relaxation for a relatively long time (compared with the atoms occupying other states).

This selectivity of SEC relaxation not only allows an accumulation of atoms in the stretched state, but also enhances their preparation in this state by speeding up the pumping of atoms occupying other states in the $F = 4$ manifold [see Fig. 3(d)]. We refer to this mechanism as SEC recycling. One can expect that increasing the atom-atom collision rate will make the recycling process even more effective (see Sec. III C). Eventually, the combined action of optical pumping and SEC puts most of the atoms in the target stretched state and leads to a significant reduction of Zeeman population in all the other states. This manifests itself as a flattening of the population gradient among nonstretched states, as shown in Fig. 3(d), and can be observed in Fig. 2(a) as a drop of most of the resonance amplitudes.

This selectivity of SEC relaxation not only allows an accumulation of atoms in the stretched state, but also enhances their preparation in this state by speeding up the pumping of atoms occupying other states in the $F = 4$ manifold [see Fig. 3(d)]. We refer to this mechanism as SEC recycling. One can expect that increasing the atom-atom collision rate will make the recycling process even more effective (see Sec. III C). Eventually, the combined action of optical pumping and SEC puts most of the atoms in the target stretched state and leads to a significant reduction of Zeeman population in all the other states. This manifests itself as a flattening of the population gradient among nonstretched states, as shown in Fig. 3(d), and can be observed in Fig. 2(a) as a drop of most of the resonance amplitudes.

For the power range 100–1000 $\mu$W the $F = 4$ resonance amplitudes level out and even tend to contract slightly for higher laser powers. We suspect that such oversaturation tendencies may indicate a coupling of the pump beam to the $F = 4$ levels despite the 9 GHz detuning.

For higher light intensities the pump beam introduces a vector light shift, which moves the position of all the resonances by the same amount without changing their separation. At the same time, the probe beam introduces a tensor light shift, which changes the separations between the individual rf resonances. For the conditions of the experiment (probe beam power about 1 $\mu$W), the tensor light shift is smaller than 1 Hz. Neither of these effects modifies the dynamics of the indirect pumping process.

Additional measurements were performed with the pump laser tuned to the $S_{1/2}F = 3 \rightarrow P_{1/2}F'$ transitions of the cesium $D_1$ line (895 nm) and similar results to those discussed above were obtained. However, due to the specific branching ratios, the hyperfine pumping on the $D_1$ transition is present even for low light intensities, while for $D_2$ excitation no optical transfer of population between the $F = 3$ and $F = 4$ manifolds is observed for such powers. Consequently, the role of spin-exchange collisions is more clearly demonstrated in the $D_2$ case and thus in this paper only excitation on the $D_2$ transition is described.

In order to obtain a direct insight into the processes described above, we converted the signals presented in Fig. 2 into sublevel populations. It may be done using the relation between the amplitude of the rf spectrum components $A^{|F,m\rangle \leftrightarrow |F,m+1\rangle}$ and the population difference in the neighboring Zeeman sublevels $m$ and $m' = m + 1$ [13,17],

$$A^{|F,m\rangle \leftrightarrow |F,m+1\rangle} = C_F[F(F+1) - m(m+1)](\rho_{(F,m+1)} - \rho_{(F,m),(F,m)}), \quad (1)$$

where $\rho$ is the density matrix. Relation (1) yields two independent sets of six (eight) equations for the seven (nine) Zeeman state populations of the $F = 3$ (4) manifold, respectively. The parameters $C_F$ represent the calibration factors that are, under our experimental conditions, different for each of the manifolds. For this reason, each hyperfine manifold is treated

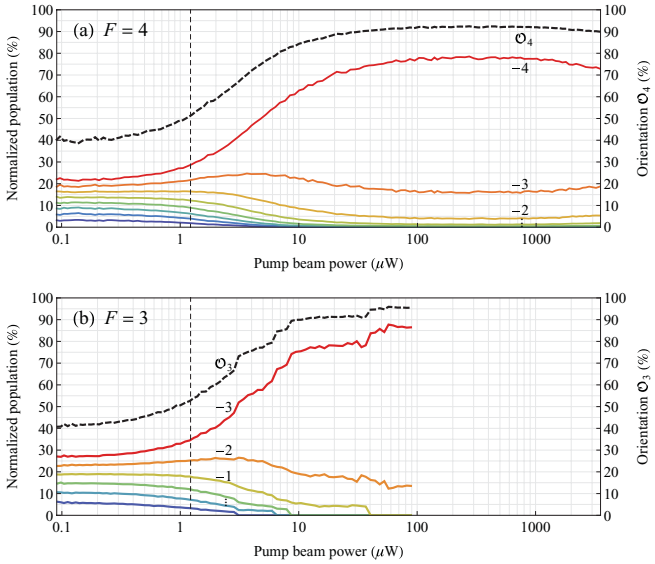


FIG. 4. (Color online) Estimated values of the populations calculated with formula (1) for (a) $F = 4$ and (b) $F = 3$ ground levels versus the pump-beam power. In the low-intensity regime the population distribution in $F = 3$ is replicated in $F = 4$ by SEC. In the high-intensity regime SEC recycling successfully promotes the stretched state population and brings down the others. Dashed lines correspond to orientation generated within a given state. No data is available for the $F = 3$ populations at high light intensities. The vertical lines are as in Fig. 2.

separately and for each of them two additional equations are needed for the set to be fully solvable. However, by restricting the calculation to relative population distribution, only one additional piece of information is required. For sufficiently strong optical pumping one can assume that the smallest population in each hyperfine manifold is equal to zero, which makes the problem tractable, albeit the solutions are not exact across the whole range of parameters.

Figure 4 presents the calculated relative population distributions for the $F = 4$ and $F = 3$ manifolds. In both cases populations are normalized to the total occupation of the manifold $\rho_{FF}$, which varies with changing strength of the optical pumping. Consequently, the plots contain information only about the relative population distribution within a given manifold, regardless of the actual population division between the manifolds. One can now calculate the orientation degree $O_F$ of each manifold $F$, which is defined as

$$O_F = \frac{1}{F}\sum_{m=-F}^{F} m\frac{\rho(F,m),(F,m)}{\rho_{FF}}. \qquad (2)$$

The atomic populations and degree of orientation are calculated based on experimental data and are shown in Fig. 4. They support the previously discussed SEC replication mechanism across the full range of available data (note the similarity of the population distributions and the orientation degrees between both manifolds). The model also reproduces the behavior characteristic for SEC recycling above 1 $\mu$W: the accelerated growth of the orientation and the related collapse

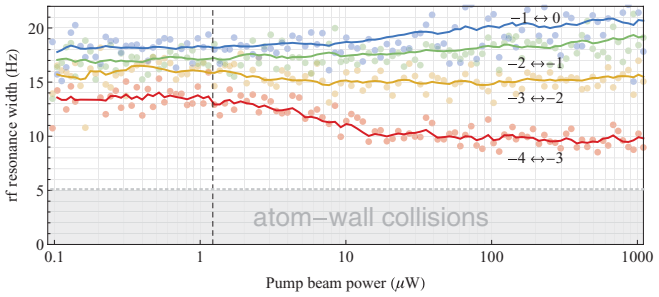


FIG. 5. (Color online) Observed widths of selected rf resonances from the $F = 4$ manifold (marked with dots). Lines were generated with exponential smoothing of the data points. The shaded region marks the value of the background-collision relaxation rate.

of all the populations except that of the stretched state in the $F = 4$ manifold.

The maximum degree of orientation obtained in the described arrangement is high. We measured the best orientation to be ∼92% [marked with a vertical broken line in Fig. 4(a)], appearing on a very broad and flat-top maximum ranging for as much as 900 $\mu$W. Observation of the very weak dependence of the orientation on the pump-beam power in the range 100–1000 $\mu$W should be helpful for obtaining a high and stable degree of orientation with a single pumping laser of modest power stability. Note that all this is achieved despite the fact that only one pump beam is used, and it is used in the configuration usually employed merely for the purpose of repumping.

### B. Resonance widths and the narrowing effect

In Fig. 5 we present the dependence of the widths (full width at half maximum, FWHM) of the four most dominant resonances of the $F = 4$ rf spectrum on the pump-light power. While Ref. [8] provides a detailed discussion of the functional form of the FWHM for particular rf resonances, we will briefly summarize the main findings. There are three major processes that contribute to the effective relaxation rate of the ground-state Zeeman-sublevel populations and increase the resonance widths.

First, collisions with the walls (referred to later as background collisions and indicated by the gray shaded region in Fig. 5) result in a relaxation rate that is independent of both atomic density and laser light power. Spin noise spectra recorded in a similar experimental configuration and extrapolated to zero atomic density (to eliminate the SEC contribution) [20] provide a value for the background-collision relaxation rate of 5.1 Hz. Secondly, the SEC are responsible for a relaxation rate that scales linearly with atomic density and also depends on the state composition of the atomic sample (in particular, it is reduced for an oriented sample). Finally, the resonances can be broadened by optical coupling to the Zeeman sublevels causing power broadening, which can arise from both the pump and the probe beams as their powers increase. Implementation of indirect nonresonant optical pumping and low probe powers ensures that the power broadening is negligible under our experimental conditions.

Figure 5 demonstrates that in the low-intensity regime the widths of different components vary between 13.5 and

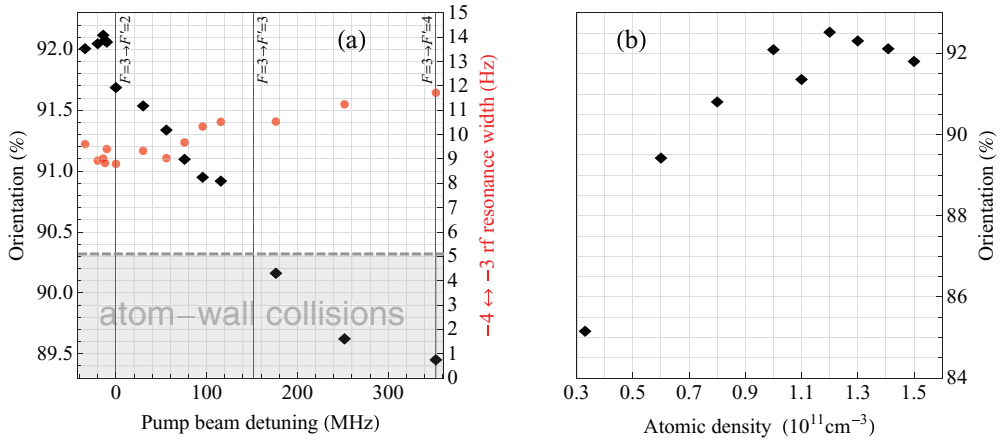


FIG. 6. (Color online) (a) Dependence of the maximal orientation in $F = 4$ (red dots) and linewidth (blue diamonds) of the rf resonance $m_F = -4 \leftrightarrow m_F = -3$ on laser detuning from the $F = 3 \rightarrow F' = 2$ transition, atomic density $1.0 \times 10^{11}$ cm$^{-3}$. The dashed line represents the FWHM in the low-intensity region. Locations of the $S_{1/2}F = 3 \rightarrow P_{3/2}F' = 2,3,4$ transitions are marked. (b) Dependence of the maximal laser-generated atomic orientation on atomic density for optimized detuning from the $F = 3 \rightarrow F' = 2$ transition.

18 Hz [12]. This is a consequence of the angular momentum conservation in SEC and results from the different number of SEC relaxation channels available for the particular sublevel population (this topic will be discussed in more detail in Sec. III D). The differences in the widths become more pronounced in the high-intensity regime, where the atomic medium approaches a high degree of orientation. We observe about 5 Hz of narrowing for the most dominant resonance, which constitutes 37% of its initial value in the low-intensity regime. This comes from the orientation buildup within the sample and is known as a light narrowing [8,14]. For the next most prominent resonance only a slight narrowing of 1 Hz is observed, while the remaining FWHM increase in the high-intensity regime.

### C. Optimizing the parameters

As was discussed in the section devoted to the high-intensity regime, the resulting degree of orientation relies substantially on the combination of pumping within the single manifold and the transfer between the $F = 3$ and $F = 4$ manifolds. The relative contributions of these two effects can be changed by varying the frequency of the pump beam. The resulting degrees of orientation in the $F = 4$ manifold obtained with different tunings that cover the whole range of the $F' = 2,3,4$ hyperfine splitting are shown in Fig. 6(a) (black diamonds).

It is observed, that tuning just below the $F = 3 \rightarrow F' = 2$ transition ($-14$ MHz) provides the best degree of orientation. Lowering the frequencies below this transition decreases the coupling to all the levels involved and results in a weaker orientation. On the other hand, moving the pump laser frequency toward the $F = 3 \rightarrow F' = 3,4$ transitions promotes pumping to the $F = 4$ manifold at the expense of the pumping within the $F = 3$ manifold. This makes the recycling process less effective and results in a lower degree of orientation. Figure 6(a) also demonstrates that the maximum narrowing correlates with the maximal orientation.

With the pump beam tuned to the optimal frequency we examined the influence of atomic density on the orientation buildup and resonance narrowing by performing the measurements in different temperatures ranging from 22 °C to 32 °C. The results presented in Fig. 6(b) show that the degree of orientation can be enhanced by 10% when raising the density from 0.3 to 1.3 $\times$ $10^{11}$ cm$^{-3}$. The atom-atom collision rate rises proportionally to the atomic density and makes the SEC recycling process more efficient, as expected. Raising the density above a certain threshold value causes other processes to emerge, such as radiation trapping [5], which could explain the efficiency saturation and falloff toward high densities.

### D. Modeling

The light-power dependence of the amplitudes of the rf resonances is modeled by calculating population distributions in the $F = 4$ and $F = 3$ states under the influence of pumping-beam and relaxation processes and then recalculated according to (1). The populations are evaluated by numerical solution of the Liouville equation for all Zeeman sublevels of the ground ($F = 3,4$) and excited ($F' = 2,3,4,5$) states. The relaxation and repopulation terms include three contributions describing the spontaneous emission, background collisions, and SEC. The background-collision contribution is described by a uniform relaxation operator of the form

$$\Gamma^{\mathrm{BCKG}}(\hat{\rho}(t)) = \tfrac{1}{2}\{\gamma\,\hat{1},\hat{\rho}(t)\}, \tag{3}$$

where the curly brackets denote the anticommutator, $\gamma$ is the rate of collisions, and $\hat{1}$ is an identity operator. SEC relaxation is described by the term

$$\Gamma^{\mathrm{SEC}}(\hat{\rho}(t)) = \tfrac{1}{2}\{\hat{\gamma}^{\mathrm{SEC}}(\hat{\rho}(t)),\hat{\rho}(t)\} \tag{4}$$

where the matrix $\gamma^{\mathrm{SEC}}$ of nonuniform values of relaxation rates is given by [21]

$$\hat{\gamma}^{\mathrm{SEC}}_{(\tilde{F},\tilde{m})}(\hat{\rho}(t)) = \gamma_0 \sum_{F} \sum_{m=-F}^{F} \rho_{(F,m),(F,m)}(t) P(\tilde{F},\tilde{m},F,m), \tag{5}$$

where the constant value $\gamma_0$ expresses the rate of atom-atom collisions in the medium and $P(\tilde{F},\tilde{m},F,m)$ are the

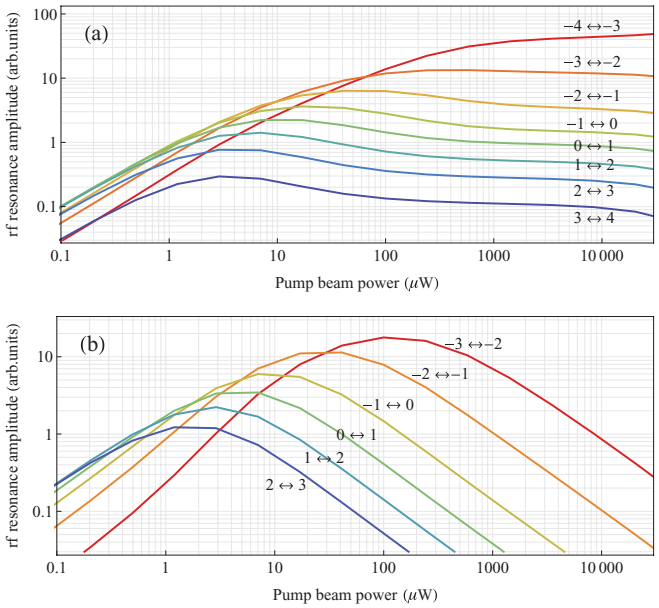


FIG. 7. (Color online) Modeled dependence of rf resonance amplitudes, $A^{|F,m\rangle\leftrightarrow|F,m+1\rangle}$, as a function of pumping-beam power.

probabilities of the $|\tilde{F},\tilde{m}\rangle$-state population loss during a collision of two atoms in states $|\tilde{F},\tilde{m}\rangle$ and $|F,m\rangle$, respectively. The procedure to calculate the $P(\tilde{F},\tilde{m},F,m)$ values is as follows. First, all possible two-body final states, i.e., states of two particles after the SEC are found assuming only the conservation of total magnetic quantum number $m_F$. All these interaction channels are assumed to have an equal likelihood (weight). Then the probability of loss of a particle in a given state is calculated accounting also for the indistinguishability of the two colliding atoms. As follows from Eq. (5) the probability of loss of the atom is a sum over each possible collision participant weighted by its concentration. It is notable that the effective spin-exchange rates $\gamma^{\mathrm{SEC}}_{(\tilde{F},\tilde{m})}$ depend on the population distribution and that they introduce a qualitatively new dynamics into the Liouville equations. The repopulation matrix is calculated in an analogous way.

This model of SEC, although being very simplified, is able to reproduce the experimental results. Indeed, it is only after the inclusion of such a form of relaxation and repopulation terms that the numerical results, shown in Fig. 7, reproduce the power dependence of the amplitudes of the measured rf resonances. In particular, the reduction of the amplitudes of the minor peaks in the high-intensity regime that we identify with the SEC recycling process is clearly visible and supports the modeling. On the other hand, simulations of the optical pumping without the SEC contribution showed that all the amplitudes grew monotonically with increasing pump power until reaching the saturation levels.

## IV. CONCLUSIONS

We have experimentally demonstrated and theoretically explained the effect of orientation buildup in the $F = 4$ cesium ground state by indirect optical pumping combined with SEC. We have shown that with optimized measurement parameters one can achieve a high level of orientation in the $F = 4$ state (up to 92%, corresponding to 78% of the population being in the $F = 4$ stretched state) in a low-density, room-temperature vapor. Standard optical pumping, which employs a circularly polarized laser beam operating on the $F = 4 \rightarrow F' = 4$ transition ($D_1$ line) causes a power broadening of the observed rf resonances that limit the measurement resolution. In contrast to that approach, the combination of indirect optical pumping and SEC results in a narrowing of the observed resonance lines. Systematic studies show that the optimized orientation is observed within a wide range of experimental parameters (laser power, detuning). The measurements were conducted under the conditions of a nonlinear Zeeman effect, which allowed resolution of individual rf resonances and a detailed analysis of the pumping and collisional dynamics by monitoring the resonance amplitudes and widths.

An agreement between the obtained theoretical and experimental population distributions supports our interpretation of the discussed distributions in terms of the SEC replication and recycling and illustrates the nonintuitive nature of atomic dynamics affected by the joint action of repopulation (indirect) optical pumping and spin-exchange collisions.

One possible application of the reported results may be for optical magnetometry. As is well known, the performance of atomic magnetometers is defined by the ratio of the signal amplitude to the resonance width. Implementation of direct pumping could potentially increase the signal amplitude but it would increase the signal width as well. Indirect pumping combined with spin-exchange collisions, however, addresses simultaneously three aspects relevant to magnetometer performance: (a) removes population from $F = 3$, (b) creates orientation in the $F = 4$ state, thus increasing the amplitude of the $m = -4 \leftrightarrow m = -3$ rf resonance, and (c) reduces the linewidth of that resonance [13]. This paves the way for the effect discussed in this paper to be implemented as an efficient alternative to the standard approach of generating the orientation by direct optical pumping [15].

## ACKNOWLEDGMENTS

The authors would like to thank Dr. J. Zachorowski for stimulating discussions. This work was funded by the UK NMS programme. Part of this work was completed within the Foundation for Polish Science Team Programme cofinanced by the EU and by the European Regional Development Fund (Polish Innovation Economy Operational Program Contracts No. POIG.02.01.00-12-023/08 and No. POIG.02.02.00-00-003/0).

[1] J. P. Wittke and R. H. Dicke, Phys. Rev. **103**, 620 (1956).
[2] K. Szymaniec, W. Chalupczak, S. Weyers, and R. Wynands, Appl. Phys. B **89**, 187 (2007).
[3] T. Weber, J. Herbig, M. Mark, N. C. Nagerl, and R. Grimm, Science **299**, 232 (2003).
[4] J. C. Allred, R. N. Lyman, T. W. Kornack, and M. V. Romalis, Phys. Rev. Lett. **89**, 130801 (2002).

[5] T. G. Walker and W. Happer, Rev. Mod. Phys. **69**, 629 (1997).
[6] M. P. Ledbetter, V. M. Acosta, S. M. Rochester, D. Budker, S. Pustelny, and V. V. Yashchuk, Phys. Rev. A **75**, 023405 (2007).
[7] W. Happer and H. Tang, Phys. Rev. Lett. **31**, 273 (1973).
[8] I. M. Savukov and M. V. Romalis, Phys. Rev. A **71**, 023405 (2005).
[9] S. Appelt, A. B. Baranga, A. R. Young, and W. Happer, Phys. Rev. A **59**, 2078 (1999).
[10] Y. Y. Jau, A. B. Post, N. N. Kuzma, A. M. Braun, M. V. Romalis, and W. Happer, Phys. Rev. Lett. **92**, 110801 (2004); I. M. Savukov, S. J. Seltzer, M. V. Romalis, and K. L. Sauer, *ibid*. **95**, 063004 (2005).
[11] M. P. Ledbetter, I. M. Savukov, V. M. Acosta, D. Budker, and M. V. Romalis, Phys. Rev. A **77**, 033408 (2008).
[12] W. Wasilewski, K. Jensen, H. Krauter, J. J. Renema, M. V. Balabas, and E. S. Polzik, Phys. Rev. Lett. **104**, 133601 (2010).
[13] B. Julsgaard, J. Sherson, J. L. Sorensen, and E. S. Polzik, J. Opt. B **6**, 5 (2004).
[14] T. Scholtes, V. Schultze, R. I. Jsselsteijn, S. Woetzel, and H.-G. Meyer, Phys. Rev. A **84**, 043416 (2011).
[15] W. Chalupczak, P. Josephs-Franks, S. Pustelny, and W. Gawlik, Phys. Rev. A **81**, 013422 (2010).
[16] G. Wasik, W. Gawlik, J. Zachorowski, and W. Zawadzki, Appl. Phys. B **75**, 613 (2002).
[17] S. Appelt, A. B. Baranga, C. J. Erickson, M. Romalis, A. R. Young, and W. Happer, Phys. Rev. A **58**, 1412 (1998).
[18] D. A. Steck, Cesium *D* Line Data (2010), [http://steck.us/alkalidata/].
[19] L. Wilmer Anderson, F. M. Pipkin, and J. C. Baird, Phys. Rev. **116**, 87 (1959); L. Wilmer Anderson and A. T. Ramsey, *ibid*. **132**, 712 (1963).
[20] W. Chalupczak and R. M. Godun, Phys. Rev. A **83**, 032512 (2011).
[21] J. Vanier and C. Audoin, *The Quantum Physics of Atomic Frequency Standards*, edited by A. Hilger (IOP Publishing, Bristol, 1989), Vol. 1.